NANO LETTERS

pubs.acs.org/NanoLett Letter

Single-Molecule Monitoring of Membrane Association of the Necroptosis Executioner MLKL with Discernible Anchoring and Insertion Dynamics

Chenguang Yang,[+] Xiaolong He,[+] Hao Wang, Zhao Lin, Wenqing Hou, Ying Lu,* Shuxin Hu,* and Ming Li

Cite This: *Nano Lett.* 2023, 23, 4770−4777 Read Online

ACCESS | Metrics & More | Article Recommendations | Supporting Information

ABSTRACT: The dynamics of membrane proteins that are well-folded in water and become functional after self-insertion into cell membranes is not well understood. Herein we report on single-molecule monitoring of membrane association dynamics of the necroptosis executioner MLKL. We observed that, upon landing, the N-terminal region (NTR) of MLKL anchors onto the surface with an oblique angle and then is immersed in the membrane. The anchoring end does not insert into the membrane, but the opposite end does. The protein is not static, switching slowly between water-exposed and membrane-embedded conformations. The results suggest a mechanism for the activation and function of MLKL in which exposure of H4 is critical for MLKL to adsorb on the membrane, and the brace helix H6 regulates MLKL rather than inhibits it. Our findings provide deeper insights into membrane association and function regulation of MLKL and would have impacts on biotechnological applications.

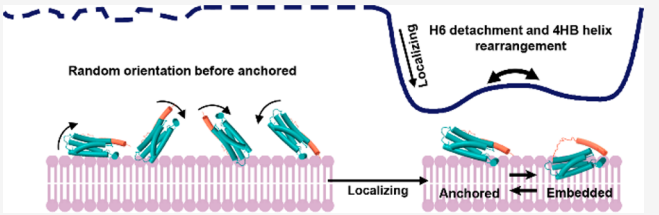

KEYWORDS: *membrane proteins, self-insertion, conformation transitions, regulation, MLKL*

Membrane proteins encoded by more than a quarter of the coding genes play important roles in a wide variety of cellular processes.[1,2] It is crucial to understand how these proteins insert and assemble in cell membranes. Many integral membrane proteins, which are usually insoluble in water, translocate across cell membranes through translocation channels such as the SecY or Sec61 complex to integrate into the lipid phase and fold into their correct structure.[3,4] Molecular mechanisms are less clear for proteins that self-insert into the membranes. This class of proteins is usually highly water-soluble and well-folded before inserting into the cell membranes to become functional.[5] The mixed-lineage kinase domain-like protein (MLKL), the most downstream effector in the pathway of necroptosis, is a particularly intriguing example of self-inserting proteins.[6−8]

MLKL comprises a C-terminal pseudokinase domain (PsKD) and a four-helix bundle (4HB) domain, bridged by a flexible brace helix region. The last two parts are also called the N-terminal region (NTR) of MLKL,[9] which plays a role in membrane rupture.[10−12] Upon initiation of the necroptotic pathway, PsKD is phosphorylated by RIP3 at Thr357 and Ser358, and the brace helices function as a device to communicate the phosphorylation events to the 4HB domain.[7,10,13] Brace helix H6 acts as a plug to prevent 4HB from inserting into the membrane before activation.[14] Because none of the α-helices in the NTR are sufficiently hydrophobic to be predicted to insert into membranes,[15] it is still under debate as to how the NTR self-inserts into membranes. The N-terminus of NTR is supposed to be the most probable insertion site because it is distant from PsKD that does not directly interact with the membranes.[16,17] Insertion of the opposite end, namely, the H4 helix-capped region, seems to be sterically hindered by PsKD. This mechanism, however, is not consistent with the result of a molecular dynamics simulation in which the N-terminus of NTR is away from the membrane surface when the H4 helix-capped region interacts directly with the membrane.[18] It can neither explain why inhibitors such as xanthine class compound 3 (Cpd3)[19] and necrosulfonamide (NSA)[20] that bind to Cys86 in the middle of helix H4 can inhibit necroptosis. One wonders which site interacts with the membrane first and which site dominates the membrane interaction.

One of the major problems in interrogating protein−membrane interactions is the lack of feasible techniques with adequate sensitivity and spatiotemporal resolution. In addition, the structure of the NTR of MLKL in membranes is still lacking. Reconstitution of NTR in membrane-mimetic liposomes, micelles, and bicelles showed release of the brace helix

Received: December 27, 2022
Revised: May 5, 2023
Published: May 16, 2023

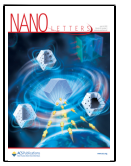

https://doi.org/10.1021/acs.nanolett.2c05062
Nano Lett. 2023, 23, 4770−4777

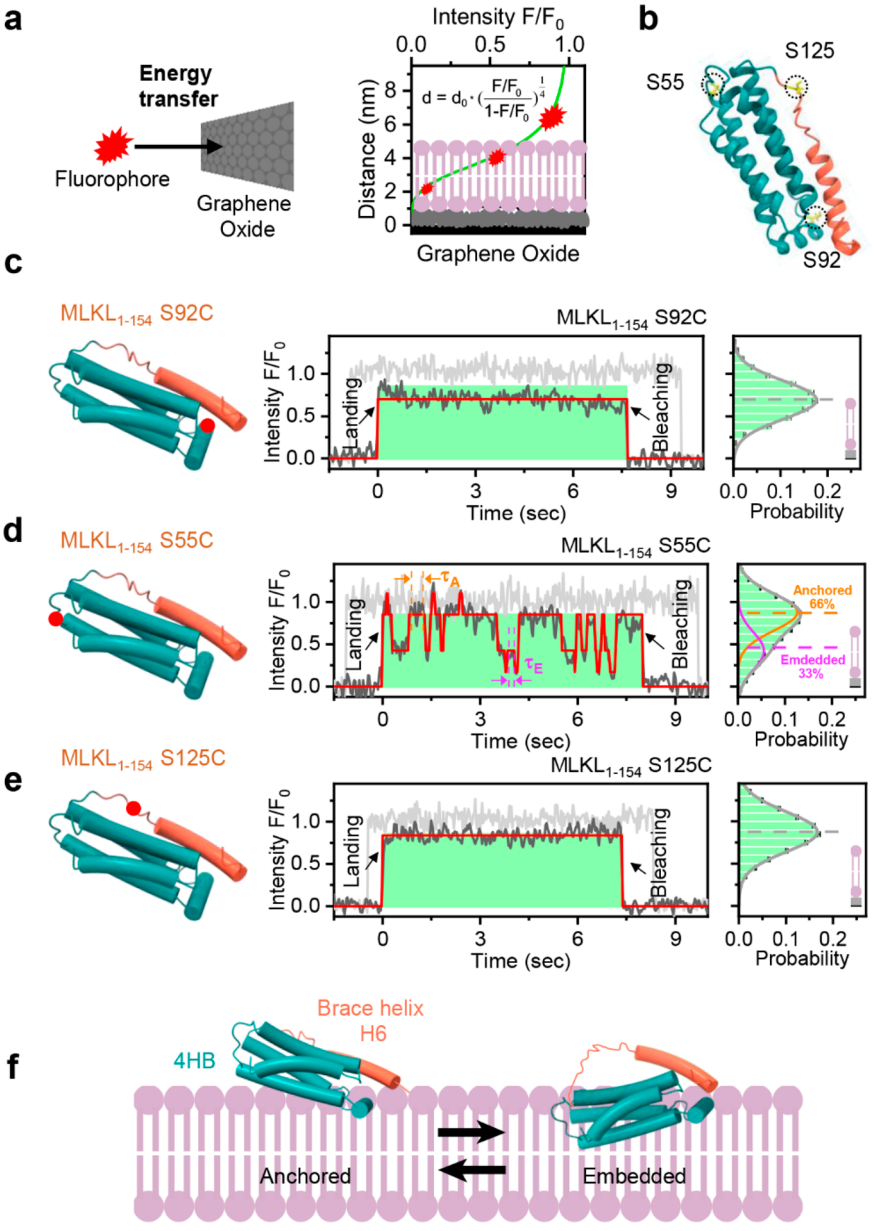

Figure 1. NTR of MLKL exhibits two membrane-associated conformations. (a) Principle of SIFA used to monitor the point-to-plane distance of a fluorophore attached to a membrane protein. (b) Structure of $MLKL_{1-154}$ with three residues (92, 55, and 125) to be labeled in the experiments. (c) Typical fluorescence trajectory (middle) and statistics of intensity (right) of S92C-labelded $MLKL_{1-154}$ (left). (d) and (e) Similar data for S55C- and S125C-labeled $MLKL_{1-154}$. The green box starts from the landing and ends with the bleaching of a fluorophore. τ_A and τ_E are the dwell times of the anchored and the embedded states, respectively. Gray lines, intrinsic fluorescence; black lines, quenched fluorescence; and red lines, HMM fitting. The statistics were from 370 trajectories. (f) Cartoon representation of the two states. It should be noted that SIFA gives only the positions of the labeled sites and that the conformations of the α-helices are only schematic. Cyan blue, 4HB; orange, brace helix H6.

region when NTR absorbs on the membrane mimics. Unfortunately, these studies did not provide further conformational information about how NTR inserts into membranes. Environment-sensitive fluorescent probe 7-nitrobenz-2-oxa-1,3-diazole (NBD) was used to gain some insights, indicating that much of the 4HB is involved in membrane insertion but not the brace helix H6.[14] However, the NBD-based method does not yield information about the insertion depth of the fluorophore in the membrane. Atomic force microscopy, optical tweezers, magnetic tweezers, and Förster resonant energy transfer (FRET) have been employed to monitor the conformational changes of single membrane proteins. However, it is difficult to detect the kinetics of self-insertion of membrane proteins. We recently developed a ratiometric technique termed surface-induced fluorescence attenuation (SIFA)[21,22] to track both axial and lateral movements of a singly labeled membrane protein in supported lipid bilayers (SLBs). Herein, we applied SIFA to study the membrane association dynamics of NTR by fluorescent labeling at strategic positions. We found that the membrane association of MLKL is dynamic and is strongly self-modulated by helix H6. More surprisingly, the membrane-insertion region of MLKL is spatiotemporally separated from its membrane-anchoring region. Our research provides new insights into the activation, membrane interaction, and modulation of MLKL.

https://doi.org/10.1021/acs.nanolett.2c05062
Nano Lett. 2023, 23, 4770−4777

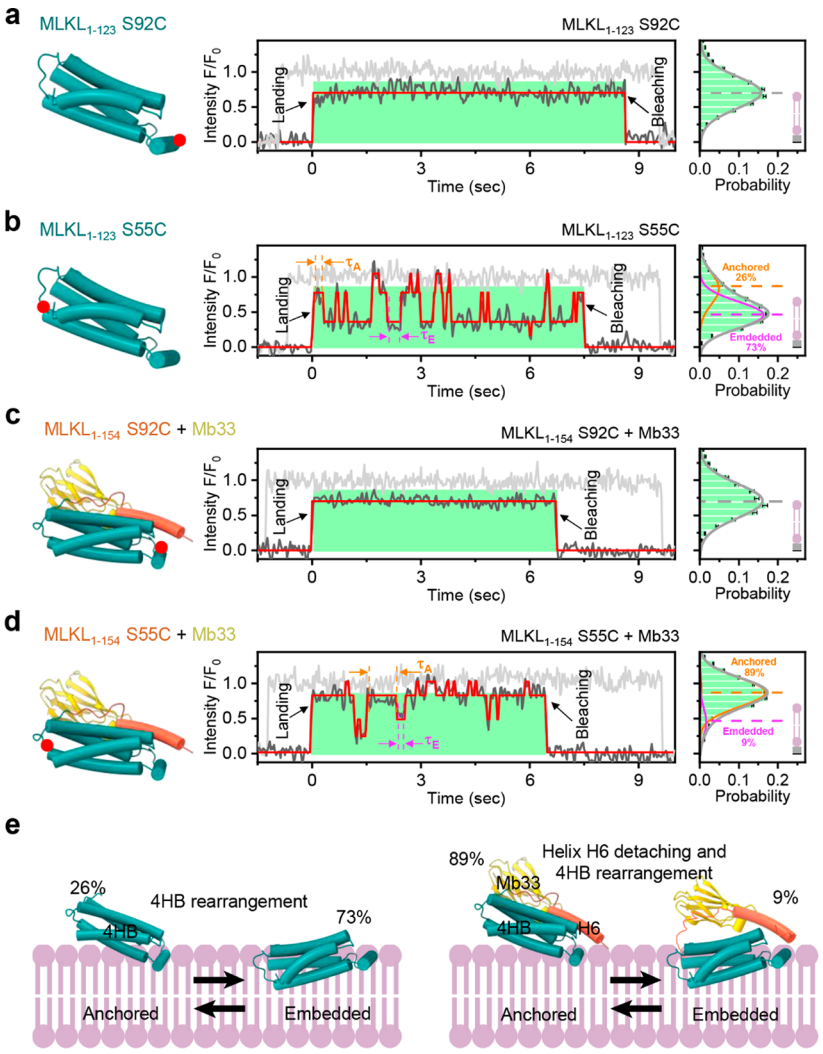

Figure 2. Brace helix H6 modulates the membrane association of MLKL. (a, b) Typical fluorescence trajectories (middle) and statistics of intensities (right) of S92C (a) and S55C (b) in $MLKL_{1-123}$. Similar data for S92C (c) and S55C (d) in the $MLKL_{1-154}$–Mb33 complex. The green box starts from the landing and ends with the bleaching of a fluorophore. Gray lines, intrinsic fluorescence; black lines, quenched fluorescence; and red lines, HMM fitting. The statistics were from 539 trajectories. (e) Cartoon representations of the two states. It should be noted that SIFA gives only the positions of the labeled sites and that the positions of Mb33 and the conformations of the α-helices are only schematic. Cyan blue, 4HB; orange, H6; and yellow, Mb33.

SIFA is based on the point-to-plane fluorescence energy transfer[23] so that it is a sensitive point-to-plane distance indicator (Figure 1a).[22] The distance d between fluorophores and the quencher layer, the single-layered graphene oxide (GO), can be calculated according to $d = d_0[(F/F_0)^{1/4}/(1 - F/F_0)^{1/4}]$, where F and F_0 are the fluorescence of fluorophores in the presence and absence of GO, respectively, and d_0 is the characteristic distance at which the energy-transfer efficiency reaches 0.5 (Figure 1a). SIFA is a powerful tool for measuring the orientation and depth of insertion of membrane proteins in SLBs produced by direct vesicle fusion on top of a GO layer modified with PEG.[24] In the present work, the NTR was site-specifically labeled with Alexa Fluo 555 at S92C on the H4 helix, at S55C in close proximity to the N-terminus of the 4HB, or at S125C in the linker between H5 and H6 (Figure 1b). We used a liposome-leakage assay to check the activity of these singly labeled MLKL samples (Figure S1). The results showed that the mutations have little impact on the liposome-leakage activity of MLKL, which is consistent with previous reports.[14] We failed to label other sites including Cys86 in NTR without disturbing its activity.

We first studied the interaction of NTR ($MLKL_{1-154}$ in this work) with SLBs composed of POPC/POPE/DOPS/PIP_2/CL/POPG (35/20/20/10/10/5) to mimic plasma membranes and mitochondrial membranes.[11,17] MLKL binds to membranes containing phosphatidylinositol 4,5-bisphosphate (PIP_2), a component of plasma membranes, or cardiolipin (CL), a component of mitochondrial membranes.[25,26] We found that PIP_2 or CL is critical for the absorption of MLKL to the lipid bilayer, consistent with the reported specificity of MLKL to PIP_2 or CL.[11,17] Three measurements were performed in parallel (Figure 1c–1e), in which the in-plane positions and the intensities of the fluorophores were recorded, yielding a 3D trajectory of the protein (Figure S2). A typical fluorescence ratio F/F_0 for S92C indicates that this site stays steadily on the bilayer (Figure 1c; intrinsic intensities in Figure S3). The F/F_0 value has a peak at 0.72 ± 0.05 (mean ± SEM) which corresponds to a distance d = 5.1 ± 0.4 nm to the GO layer. The thickness of the lipid bilayer was determined to be

https://doi.org/10.1021/acs.nanolett.2c05062
Nano Lett. 2023, 23, 4770–4777

~4.6 nm by measuring the lipid bilayer doped with fluorophore-labeled DOPE, consistent with the reported result (Figure S4).[27] Taking the thickness of the PEG cushion layer (~1 nm) into account,[28] S92C is just on top of the lipid bilayer where the headgroups of the lipid molecules are located. By contrast, the fluorescence ratio F/F_0 for S55C shows transitions among different values (Figure 1d). Two values at 0.42 ± 0.04 and 0.88 ± 0.05 are overwhelming, indicating that S55C switches mainly between ~1.0 nm above and ~1.9 nm below the surface. The S55C site may very occasionally move deeper below the surface (F/F_0 at 0.20 ± 0.04) or further above the surface (F/F_0 at 0.95 ± 0.04). We also labeled NTR at M1C which is at the N-terminal end of H1. The fluorescence trajectories for M1C are very similar to that for S55C at the linker between H2 and H3 (Figure S5). The M1C site and the S55C site are located at the same end of 4HB. The data agree with a model that the three helices do not separate when 4HB changes position in the lipid bilayer, which is supported by previous circular dichroism (CD) spectra[14,19] and NMR analysis of lipid-associated MLKL.[18,29] The results suggest that the NTR of MLKL has two dominant membrane-associated states, as illustrated by the cartoon in Figure 1f. In the anchored state, the H4-capped end is bound to the surface of the membrane while the N-terminal end is exposed to the aqueous solution. By contrast, the 4HB domain is inside the membrane in the embedded state. In both states, the residue S92C remains on the surface of the lipid bilayer so that its fluorescent intensity does not change significantly when NTR transfers between the two states, implying that the H4 helix region, in which the residue S92C is located, acts as an anchoring region. Interestingly, the fluorescence ratio F/F_0 for S125C stays steady at 0.89 ± 0.05, indicating that S125C remains essentially exposed to water despite the movements of S55C between the anchored and the embedded states (Figure 1e). This can be explained by a model in which the brace helix H6 detaches from the 4HB domain when NTR switches to the embedded state (Figure 1f). The model is in agreement with a reported mechanism in which the detachment of H6 from 4HB is essential to the activation of MLKL.[30,31]

To study the impact of H6 on the membrane association of MLKL, we monitored the interaction of the H6-deleted NTR ($MLKL_{1-123}$ in this work) with the lipid bilayer (Figure 2a, 2b, and 2e). The trajectories of F/F_0 for S92C of $MLKL_{1-123}$ resemble those of $MLKL_{1-154}$. The histogram of the ratios displays a single peak at 0.72 ± 0.05 (Figure 2a). $MLKL_{1-123}$ is therefore anchored similarly on the membrane surface. The S55C site also oscillates mainly between ~1.0 nm above and ~1.9 nm below the membrane surface during the observation, suggesting that the 4HB domain can disengage partially from the lipid bilayer by itself in the absence of H6. However, the probability of the embedded state increased from ~33% for $MLKL_{1-154}$ (Figure 1d) to ~73% for $MLKL_{1-123}$ (Figure 2b). That is, the embedded state with $F/F_0 \approx 0.42$ becomes dominant over that with $F/F_0 \approx 0.88$, indicating that $MLKL_{1-123}$ prefers the embedded state. Consistently, the characteristic dwell time of the anchored state of $MLKL_{1-123}$ (~0.17 s) is shorter than that of $MLKL_{1-154}$ (~0.66 s) (Figure S6). It is noteworthy that the characteristic dwell time of the embedded state of $MLKL_{1-123}$ (~0.51 s) is very close to that of $MLKL_{1-154}$ (~0.44 s), implying that, once embedded in the membrane, the disengagement of 4HB from the membrane is almost independent of H6. The results agree with the mechanism in which H6 detaches from 4HB before it inserts into the membrane. On the other hand, the finite probability for NTR to become embedded in the membrane indicates that H6 hinders but does not inhibit the membrane insertion of NTR.

Petrie et al. developed an inhibitor called Monobody33 (Mb33) to block the activity of MLKL by binding the NTR with nanomolar affinity.[32] The available structure of the NTR−Mb33 complex shows that Mb33 binds in the area that connects 4HB and H6 to stabilize the package of NTR (Figure S7).[32] Upon being bound by Mb33, the S92C site remains at the same position as the one in $MLKL_{1-154}$ (Figure 2c). Contrary to the case for $MLKL_{1-123}$, S55C spends more time in the anchored state (~1 nm above the surface) than it does in the embedded state (inside the membrane) (Figure 2d). The histogram of F/F_0 indicates that Mb33 tends to block the membrane insertion of NTR because the probability of the anchored state exceeds 89% according to our measurements.

We analyzed the initial conformations of the proteins. The data from the first three frames (~0.1 s; green bars) of each F/F_0 trajectory were used to build the intensity histograms to determine the initial conformations of $MLKL_{1-123}$, $MLKL_{1-154}$, and $MLKL_{1-154}$−Mb33 when they land on the lipid bilayer (Figure 3a−3c). The intensity histogram of $MLKL_{1-154}$−Mb33 (Figure 3c) indicates that the complex is all in the anchored state upon landing. The same analysis, however, indicates that the apparent probability of being anchored is only 80% for $MLKL_{1-154}$ (Figure 3b) and 56% for $MLKL_{1-123}$ (Figure 3a), respectively. We attribute these low apparent probabilities to the short dwell times of the two proteins of the anchored state. For example, the dwell time of the anchored state of $MLKL_{1-123}$ is only 0.17 s (Figure S6) such that some molecules may have changed from the initially anchored state to the embedded state within 0.1 s. In order to demonstrate this view, we plotted in Figure 3d the exponentially delaying functions of the dwell times obtained from Figure S6 and estimated the percentages of molecules that were recorded to be in the anchored state after 0.1 s. Integration from 0.1 s to infinity of the function $\exp(-t/0.17)$ yielded a value of 55%, which is the probability of $MLKL_{1-123}$ being recorded in the anchored state. Similarly, the probability was calculated to be 86% for $MLKL_{1-154}$ and 90% for $MLKL_{1-154}$−Mb33. The values all agree well with the probabilities observed in Figure 3a−3c. A similar analysis can also be applied to the data for S92C (Figure S8), supporting the view that S92C sticks steadily to the surface. Altogether, MLKL anchors on the surface immediately after it lands on the membrane. The protein is then immersed in the bilayer, switching between the anchored state and the embedded state in equilibrium (Figure S9). Taking into account the structure and the positions of the labels in the 4HB domain, our data indicate that NTR anchors on the membrane with an oblique orientation of ~70° with respect to the surface normal (Figure S10). Interestingly, the anchored conformation resembles the one suggested by Yang et al. in molecular dynamics simulations, although the details are not the same.[18] Unfortunately, their simulations were not able to show how the protein enters the membrane. Indeed, the switch from the anchored state to the embedded state is too slow to be produced by the computer simulation due to limited computational powers.

Our data revealed clearly that the self-insertion process is dynamic and reversible with an average transition rate of a few cycles per second. The state transitions mean that there is an

https://doi.org/10.1021/acs.nanolett.2c05062
Nano Lett. 2023, 23, 4770−4777

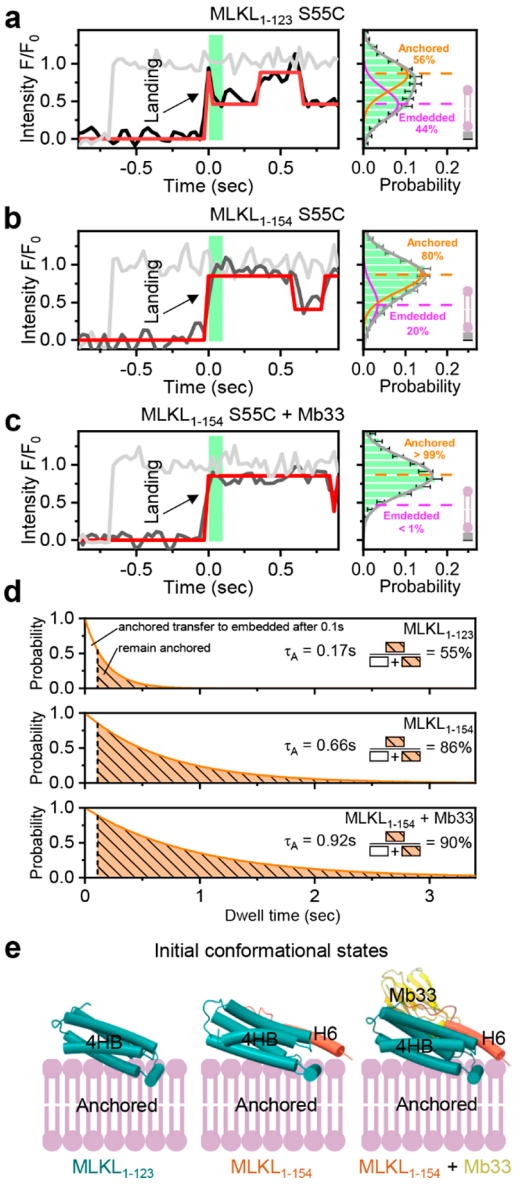

Figure 3. Initial conformation of NTR upon landing. (a−c) Trajectories (left) showing the initial fluorescence of S55C upon landing and the corresponding intensity statistics of the first three points (∼0.1 s) marked by the green bars (right). The statistics were from 370 traces. (d) Analysis of the probability of the anchored state being caught within 0.1 s (three data points) of landing, assuming an exponentially delayed distribution of the dwell times. The blank areas under the curves represent the probability that MLKL has already transferred to the embedded state after 0.1 s. (e) Cartoon representation of the initial conformations.

energy barrier between the anchored and the embedded states (Figure 4a). Theoretically, the height of the energy barrier can be given by $\Delta G = -k_BT\ \ln(-k/\upsilon)$, where k_B is Boltzman's constant, T is the temperature, k is the rate of escape from the state which equals the inverse of the dwell time, and υ is a constant that depends on the nature of the molecular dynamics.[33,34] In practice, one uses the equation only to calculate quantitatively the free-energy difference $\Delta\Delta G = -k_BT\ \ln(\tau_1/\tau_2)$, where τ_1 and τ_2 are the dwell time of the anchored and embedded states, respectively. The resulting free-energy differences between the anchored state and embedded states are $(1.0 \pm 0.2)k_BT$ for $MLKL_{1-123}$, $(-0.7 \pm 0.2)k_BT$ for $MLKL_{1-154}$, and $(-2.3 \pm 0.2)k_BT$ for $MLKL_{1-154}$−Mb33 (Figure 4b).

The 4HB domain can readily transfer between the anchored and the embedded conformations even without H6. Enhancing or reducing the H6−4HB interaction would increase or decrease the probability of anchoring against insertion. The dwell times of the embedded state of $MLKL_{1-123}$ and $MLKL_{1-154}$ are virtually the same within the experimental errors. This implies that the interaction between 4HB and membranes would become independent of H6 once it has detached from NTR.[14,29−31] As a consequence, the membrane-embedded 4HBs of both $MLKL_{1-123}$ and $MLKL_{1-154}$ have very similar structures because they both face the same hydrophobic lipid environment. Therefore, the transitions from the embedded state back to the anchored state should overcome the same energy barrier, during which 4HB would reversely undergo conformational rearrangement so that H6 can bind to 4HB again. It is reasonable to assume that H6 also detaches from NTR when the 4HB of the Mb33-NTR complex is embedded in the lipid bilayer because the insertion depth of S55C of the complex is the same as that of the NTR itself. On the other hand, Mb33 bound to H6 would assist 4HB in floating out of the membrane. The interaction between 4HB and Mb33 seems to compete with the interaction between 4HB and the membrane so that the dwell time (∼0.18 s) of the embedded state of the Mb33-NTR complex is much shorter than that (∼0.44 s) of the NTR itself (Figure S6), corresponding to a difference in the energy barriers of $(0.9 \pm 0.2)k_BT$ between the two samples (Figure 4b).

Biophysical characterization of the membrane association of MLKL is a longstanding question in necroptosis studies. In this work, we studied the dynamics of the NTR of MLKL on SLBs. We found that NTR anchors obliquely on the bilayer immediately after it lands on it. The protein is then immersed into the bilayer, a step necessary for the disruption of the cell membrane (Figure 4a). Our data suggest that the process is accompanied by the detachment of brace helix H6 from 4HB. At the same time, a structural transformation of 4HB should occur so that the hydrophobic sides of the α-helices in the 4HB domain can be exposed to the hydrophobic environment of the lipid bilayer in the embedded state. Surprisingly, we found that the anchoring end is not immersed in the bilayer but rather the opposite end, namely, the N-terminus of MLKL, is. Our data give direct evidence that exposure of the H4 helix-capped region is critical for the absorption of MLKL onto the membrane. We found that the rate of dissociation of NTR from the lipid bilayer is very low (Figure S11), meaning that MLKL would stick to and accumulate on the lipid bilayer despite the fact that 4HB can transfer back to the anchored state from the embedded state. This implicates strong interactions of the H4 helix-capped region with the membrane. A full-length structural model of the human MLKL was proposed by Arnez et al. and Petrie et al.[29,35−37] in which helix H4 is sandwiched between NTR and PsKD so that the membrane-anchoring region is sterically blocked before phosphorylation (Figure S12). A mechanism was proposed in which the phosphorylation of PsKD of the mouse MLKL unleashes 4HB to induce membrane localization and necroptotic cell death.[13] We propose that the same mechanism would be shared by the human MLKL. That is, the phosphorylation-induced exposure of H4 is the prerequisite for MLKL to be recruited to and anchored on the membrane.[38]

https://doi.org/10.1021/acs.nanolett.2c05062
Nano Lett. 2023, 23, 4770−4777

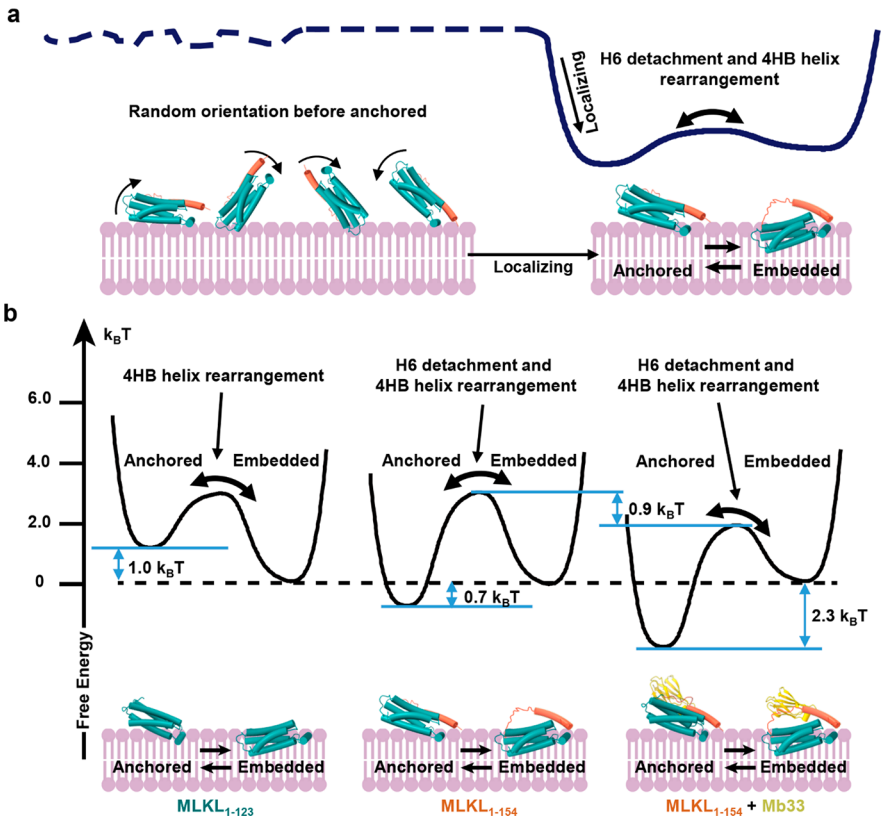

Figure 4. Dynamics of the membrane association of MLKL. (a) Cartoon representation of MLKL's landing, anchoring and self-insertion. (b) Energy landscapes of the H6-deleted NTR (left), the NTR (middle), and the NTR−Mb33 complex (right).

Our findings provide deeper insights into the membrane association dynamics of MLKL and may have impacts on biotechnological applications. The region near the H4 helix that contacts the membrane is crucial to the membrane association. This region could be the targets of drugs. In fact, the two famous necroptosis inhibitors Cpd3[19] and NSA[20] have been found to become functional by binding to Cys86 in the middle of H4. In addition, 4HB that can reversely float out of the membrane, although transiently, could be the target of future drugs, of which the inhibitor Mb33 is an excellent example. The present work reported the interaction of the NTR of MLKL with lipid bilayers in the absence of PsKD. We believe that our results captured the features of the dynamics of monomeric MLKL in membranes. NTR is widely used to study the interaction between MLKL and membranes because PsKD does not directly interact with phospholipids.[18,19,29,30,32] We did not study the interaction of oligomeric MLKL with lipid bilayers in the present work because the concentration of MLKL was set to be very low in order to observe single molecule effectively. However, we found that S55C can insert into the membrane more deeply when a mixture of labeled MLKL (1 nM) and unlabeled MLKL (50 nM) was used (Figure S13). The result supports a model in which the oligomeric MLKL may induce the rupture of membranes.[16,17] Unfortunately, the stoichiometry of the oligomers cannot be determined in such a measurement because of the presence of a high concentration of unlabeled MLKL molecules. In addition, the penetration depth of MLKL in such a measurement cannot be correctly determined because the intensity for the deeply inserted state becomes too low. At the moment, we are not able to work out a mechanism of full insertion of the oligomerized MLKL. A more profound study should be explored in the future.

■ ASSOCIATED CONTENT

Supporting Information

The Supporting Information is available free of charge at https://pubs.acs.org/doi/10.1021/acs.nanolett.2c05062.

Experimental section; liposome leakage experiments; 3D trace of MLKL protein; intrinsic fluorescence intensities; thickness of the lipid bilayer; trajectories and statistics of M1C; statistics of the dwell times; structure of the $MLKL_{1-154}$−Mb33 complex; statistics of the initial intensities of S92C-labeled samples; incubation experiments; estimation of the oblique angle; MLKL adsorption experiments; full-length model of human MLKL; and experiments under high concentration (PDF)

■ AUTHOR INFORMATION

Corresponding Authors

Ying Lu − *Beijing National Laboratory for Condensed Matter Physics, Institute of Physics, Chinese Academy of Sciences, Beijing 100190, China; University of Chinese Academy of Sciences, Beijing 100049, China; Songshan Lake Materials Laboratory, Dongguan, Guangdong 523808, China;* orcid.org/0000-0002-8421-7228; Email: yinglu@iphy.ac.cn

Shuxin Hu − *Beijing National Laboratory for Condensed Matter Physics, Institute of Physics, Chinese Academy of Sciences, Beijing 100190, China; University of Chinese*

https://doi.org/10.1021/acs.nanolett.2c05062
Nano Lett. 2023, 23, 4770−4777

Academy of Sciences, Beijing 100049, China;
Email: hushuxin@iphy.ac.cn

Authors

Chenguang Yang − *Beijing National Laboratory for Condensed Matter Physics, Institute of Physics, Chinese Academy of Sciences, Beijing 100190, China; University of Chinese Academy of Sciences, Beijing 100049, China*

Xiaolong He − *Beijing National Laboratory for Condensed Matter Physics, Institute of Physics, Chinese Academy of Sciences, Beijing 100190, China; University of Chinese Academy of Sciences, Beijing 100049, China*

Hao Wang − *Beijing National Laboratory for Condensed Matter Physics, Institute of Physics, Chinese Academy of Sciences, Beijing 100190, China; University of Chinese Academy of Sciences, Beijing 100049, China*

Zhao Lin − *Beijing National Laboratory for Condensed Matter Physics, Institute of Physics, Chinese Academy of Sciences, Beijing 100190, China; University of Chinese Academy of Sciences, Beijing 100049, China*

Wenqing Hou − *Beijing National Laboratory for Condensed Matter Physics, Institute of Physics, Chinese Academy of Sciences, Beijing 100190, China; University of Chinese Academy of Sciences, Beijing 100049, China*

Ming Li − *Beijing National Laboratory for Condensed Matter Physics, Institute of Physics, Chinese Academy of Sciences, Beijing 100190, China; University of Chinese Academy of Sciences, Beijing 100049, China; Songshan Lake Materials Laboratory, Dongguan, Guangdong 523808, China;*
orcid.org/0000-0002-5328-5826

Complete contact information is available at:
https://pubs.acs.org/10.1021/acs.nanolett.2c05062

Author Contributions

M.L., Y.L., and S.H. conceived the project. C.Y., X.H., S.H., H.W., Z.L., and W.H. performed the experiments. C.Y., Y.L., S.H., Z.L., and M.L. analyzed the data. M.L., C.Y., Y.L., and S.H. wrote the manuscript.

Author Contributions

[+]C.Y. and X.H. contributed equally to this work.

Notes

The authors declare no competing financial interest.

■ ACKNOWLEDGMENTS

This work was supported by the National Key R&D Program of China (2019YFA0709304); the National Natural Science Foundation of China (T2221001, 12090051, 11974411, 12090050, 12022409, and 32000871); the Strategic Priority Research Program of the Chinese Academy of Sciences (XDB0480000); and the CAS Key Research Program of Frontier Sciences (ZDBS-LY-SLH015). Y.L. is supported by the Youth Innovation Promotion Association of CAS (Y2021003).

■ REFERENCES

(1) Hegde, R. S.; Keenan, R. J. The mechanisms of integral membrane protein biogenesis. *Nat. Rev. Mol. Cell Biol.* **2022**, *23* (2), 107−124.

(2) Hegde, R. S.; Keenan, R. J. Tail-anchored membrane protein insertion into the endoplasmic reticulum. *Nat. Rev. Mol. Cell Biol.* **2011**, *12* (12), 787−98.

(3) Rapoport, T. A. Protein translocation across the eukaryotic endoplasmic reticulum and bacterial plasma membranes. *Nature* **2007**, *450* (7170), 663−9.

(4) Harris, N. J.; Charalambous, K.; Findlay, H. E.; Booth, P. J. Lipids modulate the insertion and folding of the nascent chains of alpha helical membrane proteins. *Biochem. Soc. Trans.* **2018**, *46* (5), 1355−1366.

(5) Liu, K. C.; Pace, H.; Larsson, E.; Hossain, S.; Kabedev, A.; Shukla, A.; Jerschabek, V.; Mohan, J.; Bergstrom, C. A. S.; Bally, M.; Schwieger, C.; Hubert, M.; Lundmark, R. Membrane insertion mechanism of the caveola coat protein Cavin1. *Proc. Natl. Acad. Sci. U. S. A.* **2022**, *119* (25), No. e2202295119.

(6) Pasparakis, M.; Vandenabeele, P. Necroptosis and its role in inflammation. *Nature* **2015**, *517* (7534), 311−20.

(7) Sun, L.; Wang, H.; Wang, Z.; He, S.; Chen, S.; Liao, D.; Wang, L.; Yan, J.; Liu, W.; Lei, X.; Wang, X. Mixed lineage kinase domain-like protein mediates necrosis signaling downstream of RIP3 kinase. *Cell* **2012**, *148* (1−2), 213−27.

(8) Martens, S.; Bridelance, J.; Roelandt, R.; Vandenabeele, P.; Takahashi, N. MLKL in cancer: more than a necroptosis regulator. *Cell Death Differ.* **2021**, *28* (6), 1757−1772.

(9) Murphy, J. M.; Czabotar, P. E.; Hildebrand, J. M.; Lucet, I. S.; Zhang, J. G.; Alvarez-Diaz, S.; Lewis, R.; Lalaoui, N.; Metcalf, D.; Webb, A. I.; Young, S. N.; Varghese, L. N.; Tannahill, G. M.; Hatchell, E. C.; Majewski, I. J.; Okamoto, T.; Dobson, R. C.; Hilton, D. J.; Babon, J. J.; Nicola, N. A.; Strasser, A.; Silke, J.; Alexander, W. S. The pseudokinase MLKL mediates necroptosis via a molecular switch mechanism. *Immunity* **2013**, *39* (3), 443−53.

(10) Davies, K. A.; Tanzer, M. C.; Griffin, M. D. W.; Mok, Y. F.; Young, S. N.; Qin, R.; Petrie, E. J.; Czabotar, P. E.; Silke, J.; Murphy, J. M. The brace helices of MLKL mediate interdomain communication and oligomerisation to regulate cell death by necroptosis. *Cell Death Differ.* **2018**, *25* (9), 1567−1580.

(11) Dondelinger, Y.; Declercq, W.; Montessuit, S.; Roelandt, R.; Goncalves, A.; Bruggeman, I.; Hulpiau, P.; Weber, K.; Sehon, C. A.; Marquis, R. W.; Bertin, J.; Gough, P. J.; Savvides, S.; Martinou, J. C.; Bertrand, M. J.; Vandenabeele, P. MLKL compromises plasma membrane integrity by binding to phosphatidylinositol phosphates. *Cell Rep.* **2014**, *7* (4), 971−81.

(12) Rubbelke, M.; Hamilton, J.; Binder, F.; Bauer, M.; King, J.; Nar, H.; Zeeb, M. Discovery and Structure-Based Optimization of Fragments Binding the Mixed Lineage Kinase Domain-like Protein Executioner Domain. *J. Med. Chem.* **2021**, *64* (21), 15629−15638.

(13) Hildebrand, J. M.; Tanzer, M. C.; Lucet, I. S.; Young, S. N.; Spall, S. K.; Sharma, P.; Pierotti, C.; Garnier, J. M.; Dobson, R. C.; Webb, A. I.; Tripaydonis, A.; Babon, J. J.; Mulcair, M. D.; Scanlon, M. J.; Alexander, W. S.; Wilks, A. F.; Czabotar, P. E.; Lessene, G.; Murphy, J. M.; Silke, J. Activation of the pseudokinase MLKL unleashes the four-helix bundle domain to induce membrane localization and necroptotic cell death. *Proc. Natl. Acad. Sci. U. S. A.* **2014**, *111* (42), 15072−7.

(14) Su, L.; Quade, B.; Wang, H.; Sun, L.; Wang, X.; Rizo, J. A plug release mechanism for membrane permeation by MLKL. *Structure* **2014**, *22* (10), 1489−500.

(15) Flores-Romero, H.; Ros, U.; Garcia-Saez, A. J. Pore formation in regulated cell death. *EMBO J.* **2020**, *39* (23), No. e105753.

(16) Chen, X.; Li, W.; Ren, J.; Huang, D.; He, W. T.; Song, Y.; Yang, C.; Li, W.; Zheng, X.; Chen, P.; Han, J. Translocation of mixed lineage kinase domain-like protein to plasma membrane leads to necrotic cell death. *Cell Res.* **2014**, *24* (1), 105−21.

(17) Wang, H.; Sun, L.; Su, L.; Rizo, J.; Liu, L.; Wang, L. F.; Wang, F. S.; Wang, X. Mixed lineage kinase domain-like protein MLKL causes necrotic membrane disruption upon phosphorylation by RIP3. *Mol. Cell* **2014**, *54* (1), 133−146.

(18) Yang, Y.; Xie, E.; Du, L.; Yang, Y.; Wu, B.; Sun, L.; Wang, S.; OuYang, B. Positive Charges in the Brace Region Facilitate the Membrane Disruption of MLKL-NTR in Necroptosis. *Molecules* **2021**, *26* (17), 5194.

(19) Rubbelke, M.; Fiegen, D.; Bauer, M.; Binder, F.; Hamilton, J.; King, J.; Thamm, S.; Nar, H.; Zeeb, M. Locking mixed-lineage kinase domain-like protein in its auto-inhibited state prevents necroptosis. *Proc. Natl. Acad. Sci. U. S. A.* **2020**, *117* (52), 33272−33281.
(20) Bansal, N.; Sciabola, S.; Bhisetti, G. Understanding allosteric interactions in hMLKL protein that modulate necroptosis and its inhibition. *Sci. Rep.* **2019**, *9* (1), 16853.
(21) Ma, L.; Hu, S.; He, X.; Yang, N.; Chen, L.; Yang, C.; Ye, F.; Wei, T.; Li, M. Detection of tBid Oligomerization and Membrane Permeabilization by Graphene-Based Single-Molecule Surface-Induced Fluorescence Attenuation. *Nano Lett.* **2019**, *19* (10), 6937−6944.
(22) Li, Y.; Qian, Z.; Ma, L.; Hu, S.; Nong, D.; Xu, C.; Ye, F.; Lu, Y.; Wei, G.; Li, M. Single-molecule visualization of dynamic transitions of pore-forming peptides among multiple transmembrane positions. *Nat. Commun.* **2016**, *7*, 12906.
(23) Hong, B. J.; An, Z.; Compton, O. C.; Nguyen, S. T. Tunable biomolecular interaction and fluorescence quenching ability of graphene oxide: application to ″turn-on″ DNA sensing in biological media. *Small* **2012**, *8* (16), 2469−76.
(24) Ang, P. K.; Jaiswal, M.; Lim, C. H. Y. X.; Wang, Y.; Sankaran, J.; Li, A.; Lim, C. T.; Wohland, T.; Ozyilmaz, B.; Loh, K. P. A Bioelectronic Platform Using a Graphene-Lipid Bilayer Interface. *ACS Nano* **2010**, *4* (12), 7387−7394.
(25) Horvath, S. E.; Daum, G. Lipids of mitochondria. *Prog. Lipid Res.* **2013**, *52* (4), 590−614.
(26) Daum, G.; Vance, J. E. Import of lipids into mitochondria. *Prog. Lipid Res.* **1997**, *36* (2−3), 103−130.
(27) Banerjee, S.; Lyubchenko, Y. L. Topographically smooth and stable supported lipid bilayer for high-resolution AFM studies. *Methods* **2022**, *197*, 13−19.
(28) Ma, L.; Li, Y.; Li, M.; Hu, S. Protein-membrane interactions investigated with surface-induced fluorescence attenuation. *Chinese Physics B* **2017**, *26* (12), 128708.
(29) Quarato, G.; Guy, C. S.; Grace, C. R.; Llambi, F.; Nourse, A.; Rodriguez, D. A.; Wakefield, R.; Frase, S.; Moldoveanu, T.; Green, D. R. Sequential Engagement of Distinct MLKL Phosphatidylinositol-Binding Sites Executes Necroptosis. *Mol. Cell* **2016**, *61* (4), 589−601.
(30) Dovey, C. M.; Diep, J.; Clarke, B. P.; Hale, A. T.; McNamara, D. E.; Guo, H.; Brown, N. W., Jr; Cao, J. Y.; Grace, C. R.; Gough, P. J.; Bertin, J.; Dixon, S. J.; Fiedler, D.; Mocarski, E. S.; Kaiser, W. J.; Moldoveanu, T.; York, J. D.; Carette, J. E. MLKL Requires the Inositol Phosphate Code to Execute Necroptosis. *Mol. Cell* **2018**, *70* (5), 936−948.
(31) McNamara, D. E.; Dovey, C. M.; Hale, A. T.; Quarato, G.; Grace, C. R.; Guibao, C. D.; Diep, J.; Nourse, A.; Cai, C. R.; Wu, H.; Kalathur, R. C.; Green, D. R.; York, J. D.; Carette, J. E.; Moldoveanu, T. Direct Activation of Human MLKL by a Select Repertoire of Inositol Phosphate Metabolites. *Cell Chem. Biol.* **2019**, *26* (6), 863−877.
(32) Petrie, E. J.; Birkinshaw, R. W.; Koide, A.; Denbaum, E.; Hildebrand, J. M.; Garnish, S. E.; Davies, K. A.; Sandow, J. J.; Samson, A. L.; Gavin, X.; Fitzgibbon, C.; Young, S. N.; Hennessy, P. J.; Smith, P. P. C.; Webb, A. I.; Czabotar, P. E.; Koide, S.; Murphy, J. M. Identification of MLKL membrane translocation as a checkpoint in necroptotic cell death using Monobodies. *Proc. Natl. Acad. Sci. U. S. A.* **2020**, *117* (15), 8468−8475.
(33) Fersht, A. R.; Matouschek, A.; Serrano, L. The folding of an enzyme. *J. Mol. Biol.* **1992**, *224* (3), 771−782.
(34) Munro, J. B.; Vaiana, A.; Sanbonmatsu, K. Y.; Blanchard, S. C. A new view of protein synthesis: mapping the free energy landscape of the ribosome using single-molecule FRET. *Biopolymers* **2008**, *89* (7), 565−77.
(35) Arnez, K. H.; Kindlova, M.; Bokil, N. J.; Murphy, J. M.; Sweet, M. J.; Guncar, G. Analysis of the N-terminal region of human MLKL, as well as two distinct MLKL isoforms, reveals new insights into necroptotic cell death. *Biosci. Rep.* **2016**, *36* (1), No. e00291.
(36) Czabotar, P. E.; Murphy, J. M. A tale of two domains - a structural perspective of the pseudokinase, MLKL. *FEBS J.* **2015**, *282* (22), 4268−78.
(37) Petrie, E. J.; Czabotar, P. E.; Murphy, J. M. The Structural Basis of Necroptotic Cell Death Signaling. *Trends Biochem. Sci.* **2019**, *44* (1), 53−63.
(38) Meng, Y.; Sandow, J. J.; Czabotar, P. E.; Murphy, J. M. The regulation of necroptosis by post-translational modifications. *Cell Death Differ.* **2021**, *28* (3), 861−883.

https://doi.org/10.1021/acs.nanolett.2c05062
Nano Lett. 2023, 23, 4770−4777